Hydrogen Generation by Ammonia Decomposition over Co/CeO2 Catalyst: Influence of Support Morphologies

Chuanqing Huang[1], Yingzhi Yu[2], Xiaoyue Tang[1], Zeyu Liu[1], Jin Zhang[1], Chuanzhen Ye[1], Yong Ye[1], and Rongbin Zhang[2]

[1]South China University of Technology
[2]Nanchang University

May 5, 2020

Abstract

Three morphology CeO2 supports with three-dimensionally ordered mesoporous structure (3DOM), nanotubes (NT) and nanocubes (NC) were synthesized by nanocasting of a mesoporous silica KIT-6 template with cubic Ia3d symmetries, hydrothermal method with and without urea, respectively, and supported cobalt catalysts were investigated on the production of COx-free hydrogen from ammonia decomposition for 300-600^{o}C. Morphological structure of CeO2 significantly influenced the catalytic activities in the ammonia decomposition, and the Co/CeO2-3DOM catalyst had a higher catalytic performance than Co/CeO2-NC and Co/CeO2-NT. It was elucidated by the formation of smaller particles size and more oxygen vacancies. The Co/CeO2-3DOM catalyst exhibited good stability and reusability at 600^{o}C for ammonia decomposition due to the three-dimensionally ordered mesoporous structure as anchoring cobalt active sites and prevention from active site aggregation. A mechanistic insight has been presented to understand the structure-activity relationship based on the structure of the CeO2 supports.

1. Introduction

Hydrogen storage technology is essentially necessary to promote renewable and clean energy with fossil fuels decreasing. Many kinds of hydrogen storage materials, such as hydrogen storage alloys, inorganic chemical hydrides, carbon materials and liquid hydrides, have been researched[1,2]. Among those hydrogen resources, the on-site generation of CO_x-free hydrogen from ammonia decomposition directly fed to proton exchange membrane (PEM) fuel cells has been especially considered[3]. This is due to ammonia converted to hydrogen and nitrogen and not produced to CO_x, which causes global warming (CO_2) and degrades cell electrodes (CO). It can be stored as liquid at 0.8 MPa (293 K), which allows for conformable, cheap and lightweight plastic tanks and a distribution network similar to that of liquefied petroleum gas (LPG). Moreover, ammonia has a high gravimetric (17.8 wt% H_2), volumetric (121 kg H_2[?]m^{-3} in the liquid form) H_2 density and energy density (3000 Wh[?] kg^{-1}). In addition, ammonia can be produced on an industrial scale through Haber-Bosch process. It is readily available, exhibits a narrow explosion limit, and decomposes relatively easily without addition of steam or oxygen[4,5]. However, ammonia as a vector for H_2 has not yet been realized largely because of the absence of an efficient, low-cost method for cracking ammonia to H_2 and N_2[6,7]. Therefore, development of catalysts to efficiently attain hydrogen by on-site generation from ammonia at low temperature is critically important for mobile and remote applications.

Nowadays, many works have been devoted to exploit efficient catalysts for ammonia decomposition. Currently, various metals and mixed metal oxides (such as Ru[8], Ni[9], Fe[10], Co[11], Cu[12], Ni-Fe[13], Co-Mo[14], Fe-Co[15], etc.) and compounds[16,17]have been tested for ammonia decomposition. Ru is the most active metal, but this

noble metal is very expensive and thus limits its large-scale application. Therefore, using a non-noble metal to replace Ru metal is necessary for practical applications. Amongst these Ni-, Co- and Fe-based catalysts, the nitrogen biding energy of cobalt is the closest one to the optimum value range[18]. Lendzion-Bielun et al.[19] reported that Co was more effective than the iron catalyst in the ammonia decomposition. Zhang et al.[20] reported that Co/MWCNTs catalysts after pretreatment in nitrogen exhibited high catalytic activity for ammonia decomposition. However, the multi wall carbon nanotubes (MWCNTs) is easily methanation in high temperature under hydrogen atmosphere. Therefore, the development of highly active and carbon resistant Co-based catalysts for ammonia decomposition becomes a major aspect of research in this field.

In the past years, three-dimensionally ordered mesoporous (3DOM) materials have been intensively investigated for the applications in various fields (such as semiconductors, photonics, electrochromics, and catalysis[21]). Usage of CeO_2 as catalyst, catalyst support, or catalyst promoter has been widely reported due to its unique redox properties and remarkable oxygen storage capacities[22]. For example, the addition of CeO_2 to nickel catalysts was reported to improve the catalytic activity[23]. 2D ultrathin MoS_2 nanosheets grown on uniform CeO_2 hollow spheres were reported by Gong et al.[24] for enhancing activity in catalytic ammonia decomposition for H_2production. Llorca et al.[25] performed an in situ X-ray photoelectron spectroscopy (XPS) study of CeO_2-supported Ni and Ru catalysts under ammonia decomposition conditions to get an insight into the nature of the active sites. Moreover, CeO_2 with different morphologies by precise control of surface atomic arrangements can modify the reactivity of Ce^{4+}/Ce^{3+} ions, influencing the formation of oxygen vacancies, which, in turn, affects the catalytic performance[26-29]. However, the effects of morphologies on CeO_2 support with three-dimensional order mesoporous structure, nanocubes and nanotubes in the ammonia decomposition have not been investigated.

Therefore, three different morphologies of CeO_2 with three-dimensional ordered mesoporous, nanocubes and nanotubes were designed as the support for ammonia decomposition to evaluate the morphology-dependent ammonia decomposition activity in this research. Meanwhile, N_2 physisorption (BET), transmission electron microscopy (TEM), X-ray power diffraction (XRD), temperature-programmed reduction of hydrogen (H_2-TPR) and temperature-programmed desorption of carbon (CO-TPD) were used to reveal the catalyst structure-performance relationship.

2. Experimental

2.1 catalyst preparation

All the chemicals reagents used in our experiments, except for Pluronic P123 ($EO_{20}PO_{70}EO_{20}$, Aldrich), were purchased from Sinopharm Chemical Reagent Co., Ltd (analytical grade) and used without further purification. Highly ordered mesoporous silica with cubic Ia3d symmetry (designated as KIT-6) was prepared by a template method according to the literature[30]. In a typical synthesis process, 6 g Pluronic P123 was dissolved in 217 g de-ionized water and 11.8 g of conc. HCl (37%) and stirred over night at 35^{o}C. 6 g n-butanol was added. After 1 hour of stirring, 12.9 g of TEOS (Aldrich 98%) was quickly added and stirred for 24 h at 35^{o}C. The milky suspension was transferred to a Teflon-lined stainless steel autoclave and annealed at 100^{o}C for 24 h. The solid product was filtered, washed with an ethanol-HCl mixture. The sample was dried at 100^{o}C and calcined at 550^{o}C for 5 h to completely eliminate the template. The white KIT-6 powder (2 g) was obtained.

Three-dimensionally ordered mesoporous $CeO_2$was fabricated using KIT-6 as hard template. Typically, proper amounts of $Ce(NO_3)_3{\cdot}6H_2O$ was dissolved in 15 mL of ethanol stirring at room temperature, followed by the addition of 0.5 g of KIT-6 after complete dissolution. After sonicated for 10 min, the precursor@KIT-6 composite was stirred at room temperature until a nearly dry powder, and then dried and calcined at 600^{o}C in air atmosphere for 4 h with a heating rate of 1^{o}C/min. To remove the silica template, the resulting sample was treated with a hot aqueous solution of 2M NaOH, and then centrifuged and washed with distilled water and ethanol several times, and eventually dried at 100^{o}C. The product (0.7 g) was denoted as CeO_2-3DOM.

The CeO_2-nanotube (CeO_2-NT) was prepared by a hydrothermal method according to the literature[31]. The synthesis process was as follows: under vigorous stirring, $Ce(NO_3)_3{\cdot}6H_2O$ (3.4g) was dissolved in 160 mL

distilled water, and then urea (7.2g) was added. The mixture was transferred to a 200 mL Teflon-lined stainless-steel autoclave and held in 80^{o}C for 24 h in an electric oven for 5 h. After the autoclave was cooled to room temperature, fresh precipitates were separated by centrifugation, washed with deionized water. The $Ce(OH)CO_3$ was obtained after drying the precipitates at 80^{o}C in air overnight. The $Ce(OH)CO_3$(0.5g) was dissolved in 80 mL NaOH (2.4M) solution and then sequentially stirred for 30 min. The mixed solution was transferred into a 100 mL Teflon-lined autoclave and maintained at 120^{o}C for 48 h. After the autoclave was cooled to room temperature, fresh precipitates were separated by centrifugation, washed with deionized water. The fresh precipitates were dried in air at 80^{o}C overnight to obtain faint yellow CeO_2-NT powder (0.4 g).

The CeO_2-cubes (CeO_2-NC) were obtained in a similar procedure in our previous work[27,32]. Briefly, $Ce(NO_3)_3{\cdot}6H_2O$ (1.72g) were dissolved in 20 mL distilled water under vigorous stirring for 30 min and then added 60 mL NaOH (10M) solution to form a milky slurry. The mixture was transferred into a 100 mL Teflon-lined stainless-steel autoclave and held in 130^{o}C for 48 h in an electric oven. After hydrothermal treatment, the suspension was filtered and the solid residue was washed with distilled water, dried at 100°C overnight to obtain CeO_2-NC sample (0.5 g).

The support materials of CeO_2-3DOM, CeO_2-NC and CeO_2-NT were successively impregnated with an ethanol aqueous solution of $Ce(NO_3)_3{\cdot}6H_2O$. The products were evaporated in vacuum conditions and dried in an oven at 60^{o}C and calcinated at 600^{o}C for 2 h in air atmosphere. The Co loading amount for Co/CeO_2-3DOM, Co/CeO_2-NC and CeO_2-NT catalysts was fixed at 5 wt%. The CeO_2 with different morphology supported Co catalysts for ammonia decomposition to hydrogen is illustrated in Scheme 1.

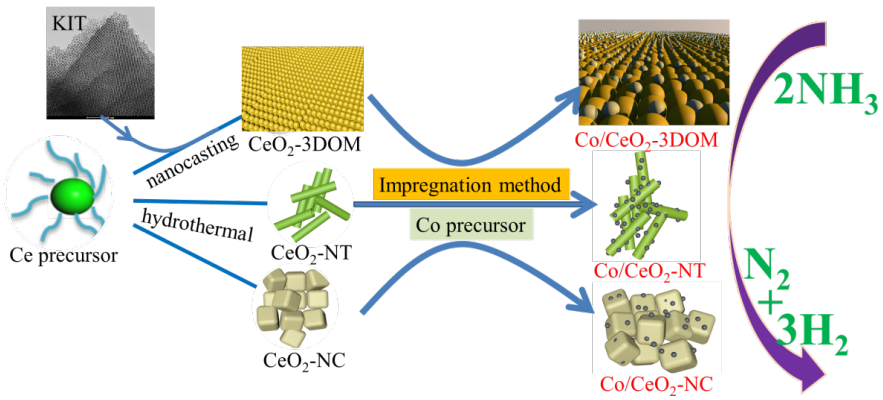

Scheme 1. Schematic diagram to illustrate the CeO_2 with different morphology supported Co catalysts for ammonia decomposition to hydrogen.

2.2 Catalyst characterization

X-ray diffraction (XRD) measurement was carried out for the prepared catalysts on a Bruker AXS D8 Focus diffractometer operated with Cu Kα (λ =0.154056 nm) radiation at 40 kV and 30 mA with 3 mm scattering scale. Diffraction data (2ϑ = 10-80^{o}) were collected at a scanning rate of 4^{o}/min. The Scherrer equation (1) was used to determine the crystal size of different phases based on the most intense diffraction peaks for CeO_2(111) and Co_3O_4 (311).

$$D = \frac{k}{\cos} \quad (1)$$

Where k is the Scherrer constant, β is full width at half of the maximum intensity, and ϑ stands for the diffraction angle.

The surface area and pore size distributions of bare CeO_2 support as well of Co/CeO_2catalysts were determined by N_2 adsorption/desorption isotherms at -196^{o}C in a Micromeritics ASAP2020 equipment (Micro-

meritics, USA). All the samples were treated at 200^{o}C for 5 h under vacuum ([?] 1 μm Hg), The surface area was calculated using the Brunauer, Emmett and Teller (BET) method. The pore size distribution was determined by the Barrett, Joyner, and Halenda (BJH) method.

A transmission electron microscope (TEM, JSM-2010, JEOL, Japan) was used for imaging of the samples, The powders were suspended in ethanol for 30 min under ultrasonic treatment before they were deposited onto the carbon-film-coated copper grids.

Reducibility of the catalysts was determined by H_2-TPR (Temperature-programmed reduction of hydrogen) using a Micromeritics 2920 system (Autochem II, Micromeritics, USA) equipped with a TCD detector and quartz tubular reactor. 50 mg of catalyst was used. Before the H_2-TPR analysis, in order to remove the absorbed impurities (e.g. H_2O), the samples was degassed at 200^{o}C under a Ar flow (30 mL/min) for 1 h. After the sample was cooled to RT, the H_2-TPR was then introduced under flow of 10% H_2 in Ar (30 mL/min) from 50^{o}C to 800^{o}C with a ramp of 10^{o}C/min. The amount of H_2 uptake during the reduction was recorded by TCD detector.

Temperature-programmed desorption of CO (CO-TPD) was performed on a reactor with the same equipment of TPR detection to measure the exposed Co surface area. The catalyst (50 mg) was loaded into a 1/4 inch quartz tube for each test. Prior to the pulse CO chemisorption measurement, the catalyst was reduced at 600^{o}C for 2 h in 10% H_2(balance with Ar), and then cooled down to room temperature in He flow. Then, the 10% CO/He flow was introduced for a period of 0.5 h at RT. After CO chemisorption was performed under cryogenic conditions, pure He was introduced to remove redundant CO. Heating were performed with a 10oC/min ramp from room temperature to 800oC. CO uptake was measured using a gas chromatography equipped with TCD detector. Co metal surface area was calculated by assuming a stoichiometry of 1:1 for CO:Co.

X-ray photoelectron spectroscopy with an ESCALAB250 Xi system (XPS, Thermo Fisher Scientific, USA) was used to determine the binding energies (BEs) of Co 2p, O 1s and Ce 3d of surface species, using monochromatic AlKa (1486.6 eV) as excitation source. Spectra were registered at ambient temperature in a vacuum (residual pressure $< 10^{-7}$ Pa). The binding energy of C 1s (284.8 eV) was used as a reference. After subtraction of the Shirley-type background in the XPS PEAK program, the spectra was fitted by the Gaussian function. The surface composition and chemical state were evaluated based on the areas and binding energies of the Ce 3d, Co 2p and O 1s photoelectron peaks.

2.3 Catalytic activity measurements

Catalytic activities were evaluated in a quartz tube fixed bed reactor with the inner diameter of 6 mm under pure ammonia (atmospheric pressure, GHSV= 6000 mL/g_{cat}*h). Prior to reaction, the synthesized catalysts (100 mg) were in-situ reduction by a pure H_2 flow at 600oC for 2 h. Then the temperature was decreased to 300oC under Ar flow. After the residual hydrogen was removed, the gas was switched to ammonia. The reaction temperature was raised from 300oC to 600oC with a 50oC interval. The inlet flow rate of ammonia and hydrogen was read from the mass flow controller. On-line gas chromatography (GC-9790II, Zhejiang FULI Analytical Instrument Co., Ltd., China) which equipped with a TCD detector and Poropak N column using Ar as carrier gas, was used to analyze the gas composition. The total amount of ammonia in feed gas and unconverted amount of ammonia were denoted as $A_{NH_3,in}$and $A_{NH_3,out}$, respectively. The conversion of ammonia (X_{NH_3}) was calculated using the following equation:

$$X_{NH_3}=\frac{(A_{NH_3,in}-A_{NH_3,out})}{A_{NH_3,in}}\times 100\% \quad (2)$$

In the desired temperature value, all of the data were done in triplicate after the reaction reached steady state. The H_2 formation rate was calculated from the equation (3), where V_{NH3} refers to amount at a flow rate by mass flow meter, as follow:

$$H_2 \text{ formation rate (mmol /min• } g_{cat}) = \frac{\frac{V_{NH_3}}{22.4}.Conv_{(NH_3)}\%.1.5}{m_{cat}} \quad (3)$$

3. Results and discussion

3.1 Characterization

3.1.1 XRD

Fig. 1 shows the powder XRD pattern of the as-prepared CeO_2 supports and the corresponding supported Co catalysts. As shown in Fig. 1a and Fig. 1b, high-intensity peaks at $2\vartheta = 28.6^{o}$, 32.9^{o}, 47.5^{o}, 56.3^{o}, 59.1^{o}, 69.4^{o}, 76.7^{o}, and 79.1^{o}, corresponding to (111), (200), (220), (311), (222), (400), (331) and (420) planes, can be indexed to the face-centered cubic fluorite-structure with space group Fm-3m. Mean crystallite size, as calculated by Scherrer equation, was 12.7 nm for the CeO_2-3DOM, 23.2 nm for the CeO_2-NC, and 10.9 nm for the CeO_2-NT. When Co was added to CeO_2, the structural characteristic peak of position and intensity of bare CeO_2 did not modify notably, indicating that the crystallite size and the lattice constant of CeO_2 remain almost constant. However, the diffraction peak at 37.1^{o} in Fig 1b was the typical reflection of Co_3O_4 (311), indicating that Co_3O_4 has formed after calcination treatment for Co/CeO_2 catalysts. The crystalline size of Co_3O_4 sequence was Co/CeO_2-NC (39 nm) > Co/CeO_2-3DOM (33 nm) > Co/CeO_2-NT (19 nm).

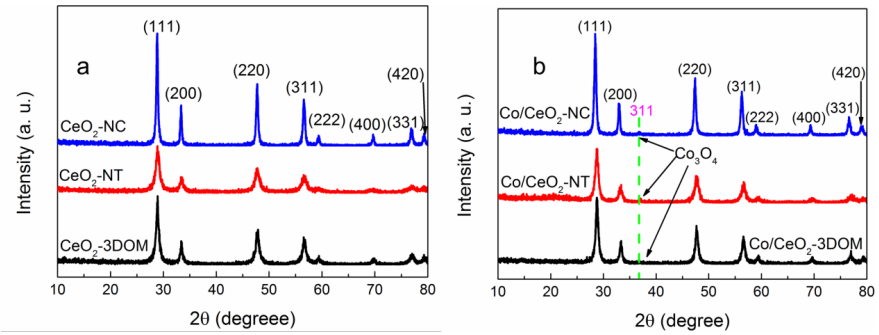

Fig. 1. XRD patterns of (a) CeO_2-3DOM, CeO_2-NC, CeO_2-NT supports and (b) Co/CeO_2-3DOM, Co/CeO_2-NC, Co/CeO_2-NT.

3.1.2 N_2 sorption

The N_2 adsorption-desorption isotherms of the as-prepared KIT-6, CeO_2 supports and Co/CeO_2 with different morphologies were shown in Fig. 2. According to the IUPAC classification, type IV isotherms with a H1 hysteresis loop were observed in Fig. 2a. Physical properties like specific surface area (S_{BET}), pore volume (V_t) and pore diameter (d_{BJH}) of the synthesized materials were summarized in Table 1. The KIT-6 synthesized by hydrothermal reaction at 100^{o}C had a BET surface area of 1243 m^2/g, high pore volume of 1.53 cm^3/g and average pore size of 6.7 nm. It indicates that calcined *Ia3d*silica (KIT-6) has formed the large channel-like pores in narrow range of size. TEM images of KIT-6 (Fig. 5a and Fig. 5b) directly demonstrated its structure of well-ordered and alternative pore channels.

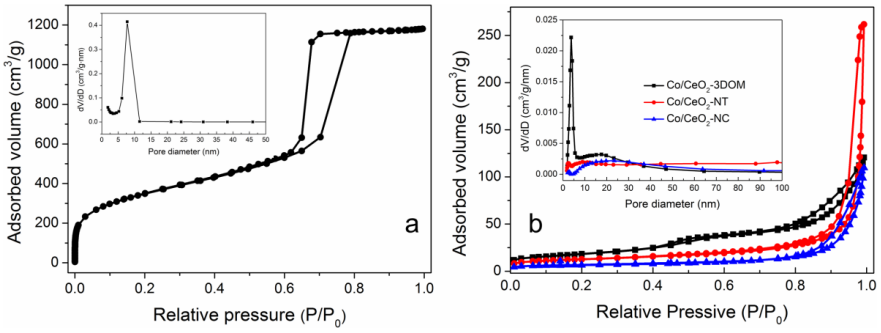

As shown in Fig.2b, the adsorption-desorption isotherms of Co/CeO_2-NC and Co/CeO_2-NT catalysts were

type IV with a H3 hysteresis loop. For Co/CeO_2-NT catalyst, the adsorbed volume within a pressure range about $0.8 < P/P_0 < 1$ was 260 cm^3/g. This is ascribed to the capillary condensation as the adsorption of the nitrogen molecules sharply increases. For Co/CeO_2-3DOM catalysts, the adsorption-desorption isotherms was type IV with type H1 and H2 hysteresis loops within the specific pressure ranges ($0.4 < P/P_0 < 0.7$ and $0.8 < P/P_0 < 0.1$, respectively). It indicates that there exists well-developed mesopores in the prepared Co/CeO_2-3DOM catalysts. Compared with the CeO_2-3DOM in Table 1, the surface areas and pore volumes of the supported catalysts were all decreased after the metal loading. This means that Co species have been incorporated into the pore of the mesoporous CeO_2-3DOM.

Fig. 2. N_2 physisorption isotherm of (a) KIT-6 and (b) Co/CeO_2-3DOM, Co/CeO_2-NC, Co/CeO_2-NT at -196ºC. Pore size distribution from BJH desorption (Inset) of (a) KIT-6 and (b) Co/CeO_2-3DOM, Co/CeO_2-NC, Co/CeO_2-NT.

Table 1. Physical of properties of KIT-6, Co/CeO_2-3DOM, Co/CeO_2-NC, Co/CeO_2-NT catalysts.

Samples	CO-uptake ($10^{-3}\times$mmol/g_{cat})[a]	H_2 formation rate ($10^{-3}\times$mmol/min·g_{cat})[b]	TOF_{H2} (min^{-1})[c]
Co/CeO_2-3DOM	469.1	596.8	1.27
Co/CeO_2-NC	464.0	526.8	1.14
Co/CeO_2-NT	468.5	304.0	0.65

3.1.3 H_2-TPR

The H_2-TPR spectra of CeO_2 support and Co/CeO_2 in Fig. 3 were utilized to examine the strength of interaction between active component and support. For three CeO_2 supports, the temperatures of 250ºC-400ºC and 400ºC-600ºC represent the reduction of ceria surface oxygen with the formation of Ce^{3+} species and an oxygen lacuna on subsurface, respectively. The reduction temperature of 600ºC-1000ºC can remove bulk oxygen from the ceria structure along with the reduction of Ce^{4+} into Ce^{3+}ions[33,34]. However, compared with CeO_2-NC and CeO_2-3DOM, the reduction peak of CeO_2-NT was weak, indicating that surface capped oxygen of ceria is little.

The reduction of nano Co_3O_4 takes place as a two-step reduction process at 320ºC and 400ºC via Co_3O_4 - CoO - Co^{035}. Co/CeO_2-NT (273oC and 288oC), Co/CeO_2-NC (251oC and 271oC) and Co/CeO_2-3DOM (311oC and 362oC) catalysts have two reduction peaks. The low temperature section belongs to the Co^{3+} to Co^{2+}. The high temperature section is assigned to Co^{2+} to Co^0. Obviously, the doped cobalt ions in these catalysts exist in mixed oxidation states (Co^{3+} and Co^{2+}), which is confirmed by the results of XRD characteristic and XPS investigations. Compared with the reduction peak of pure Co_3O_4, the reduction peak of Co/CeO_2-NT, Co/CeO_2-NC and Co/CeO_2-3DOM catalysts systematically shifted to the lower temperature side. It indicates that the reducibility is promoted by the electronic metal-support interaction (EMSI). Compared to Co/CeO_2-3DOM catalyst, Co/CeO_2-NC and Co/CeO_2-NT catalysts had lower reduced peak temperature, indicating that the electron metal-support interactions (EMSI) of Co/CeO_2-NT and Co/CeO_2-NC catalysts are weaker than that of Co/CeO_2-3DOM catalyst. As such, this strong Ce-O-Co bond causes more electrons transfer from Co to the support, thus forms Co^{n+}. As a consequence, the area ratio of the reduction peaks roughly represents the relative number of Co^{n+}. Based on TPR peaks area, the order of H_2 consumption was obtained: Co/CeO_2-3DOM (0.80 mmol/g_{cat}) > Co/CeO_2-NC (0.79 mmol/g_{cat}) > Co/CeO_2-NT (0.72 mmol/g_{cat}), which is in accordance with the catalytic activity results obtained from Fig. 7.

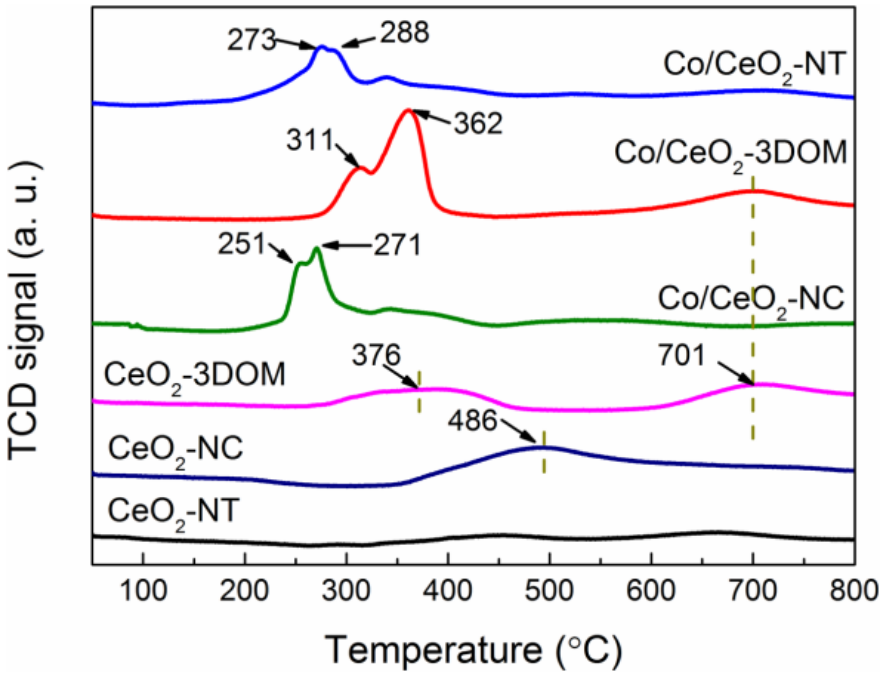

Fig. 3. TPR profiles of CeO_2-3DOM, CeO_2-NC, CeO_2-NT supports, Co/CeO_2-3DOM, Co/CeO_2-NC and Co/CeO_2-NT catalysts.

3.1.4 CO-TPD

Fig. 4 illustrated the desorption behavior of CO from the Co catalysts. The maximum desorption peak temperature for Co/CeO_2-NC, Co/CeO_2-NT and Co/CeO_2-3DOM catalysts were 102ºC, 86ºC and 98ºC, respectively. Based on the peak area of CO-TPD profiles and assumption of an adsorption of one per metal atom[36], the CO absorption value of Co/CeO_2-3DOM, Co/CeO_2-NC and Co/CeO_2-NT catalysts were 0.4691 mmol/g, 0.4640 mmol/g and 0.4684 mmol/g, respectively. The Co metal dispersion of Co/CeO_2-3DOM, Co/CeO_2-NC and Co/CeO_2-NT catalysts were 55.4%, 54.7% and 55.3%, respectively. The turnover frequency of H_2 formation (TOF_{H2}) was calculated by the H_2 formation rate (mmol/min·g_{cat}) to the number of exposed Co surface atoms per gram of catalyst[37]. As shown in Table 2, the TOF_{H2} of Co/CeO_2-3DOM catalyst (1.27 min^{-1}) was higher than that of Co/CeO_2-NC (1.14 min^{-1}) and Co/CeO_2-NT catalyst (0.65 min^{-1}).

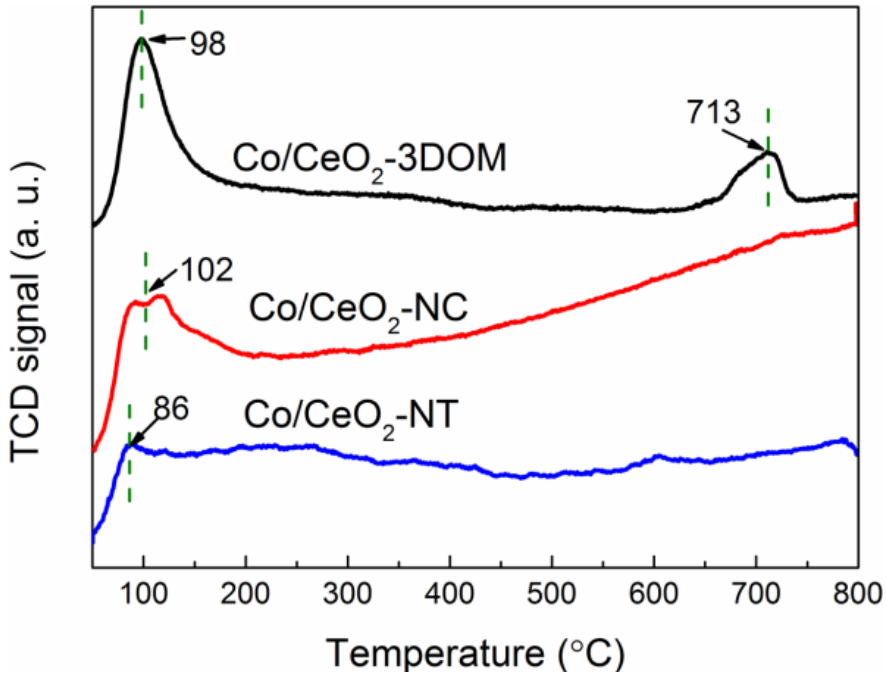

Fig. 4. CO-TPD profiles of Co/CeO_2-3DOM, Co/CeO_2-NC and Co/CeO_2-NT catalysts.

Table 2. CO-uptake, H_2 formation rate and TOF values of the as-prepared samples for ammonia composition at 350^{o}C.

[a] The absorbed CO values of the samples are calculated on the basis of the peak areas of CO-TPD.

[b] The H_2 formation rate of prepared catalysts are calculated by Eq. (3) at 350^{o}C.

[c] The TOF_{H2} values of prepared catalysts are calculated according to the original data provided by the temperature of 350^{o}C, the H_2 formation rate (mmol/min·g_{cat}) by the composite catalysts per second and the number of surface of Co atoms determining by CO-TPD[37].

3.1.5 TEM

The TEM images of the prepared KIT-6, Co/CeO_2-3DOM, Co/CeO_2-NC and Co/CeO_2-NT catalysts were shown in Fig. 5 to assess the morphology. As seen from Fig.5a and Fig. 5b, the prepared KIT-6 template exhibited a well-ordered and alternative pore channel structure (7.5 nm pores size). The CeO_2support could be a very effective replica of the KIT-6 structure to form a three-dimensional ordered mesoporous structure (Fig. 5c). These observations are consistent with the (BJH) pore size distributions determined from the desorption branch exhibited in Fig. 2 and Table 1. The mean diameter of CeO_2 nanotubes was around 34.5 nm in Fig. 5i. For CeO_2-NC supports, the diameter was a size ranging from 13.1 nm to 37.6 nm in Fig. 5e. The average diameter sizes of observed cobalt nanoparticles for Co/CeO_2-NT (Fig. 5i) and Co/CeO_2-NC (Fig. 5h) catalysts were 6.6 nm and 7.8 nm, respectively. While for Co/CeO_2-3DOM, the average diameter size of these particles was 5.2 nm.

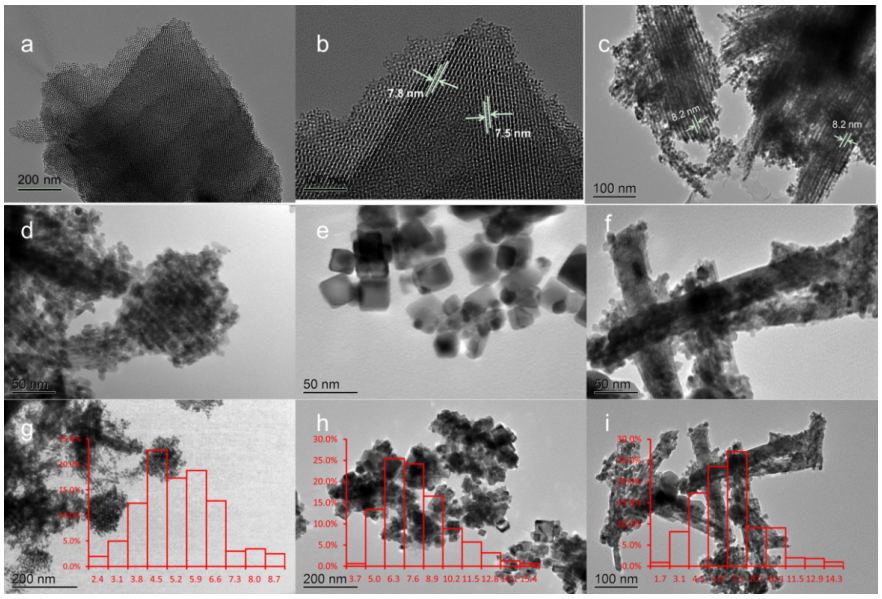

Fig. 5. TEM images of KIT-6 (a, b), CeO_2-3DOM (c), Co/CeO_2-3DOM (d, g), Co/CeO_2-NC (g, h) and Co/CeO_2-NT (f, i).

3.1.6 XPS

The surface chemical composition of Co/CeO_2 catalysts in the Fig. 6 were identified by XPS. As for Fig. 6a, the XPS survey spectrum revealed the dominated presence of Ce, Co and O elements in the catalyst surface. Fig. 6b showed that the XPS spectra of Ce 3d for all the investigated samples fitted well to eight deconvoluted peaks at 882.5, 884.7, 888.6, 898.4, 900.9, 902.2, 907.5 and 916.6 eV. Peaks of 884.7 and 902.2 eV could be ascribed to Ce^{3+}3d, the remaining peaks could be attributed to Ce^{4+}3d[32,38]. These results indicate the coexistence of Ce^{3+} and Ce^{4+} species on the surface of three catalysts. The Ce^{3+}/Ce^{4+} ratio of Co/CeO_2-3DOM (0.53) was higher than that of Co/CeO_2-NC (0.39) and Co/CeO_2-NT (0.33) catalysts. Due to the presence of larger Ce^{3+} ions (ionic radius 1.143Å) replacing smaller Ce^{4+} ions (0.970Å), this result shows that the increasing lattice parameter and oxygen vacancies can be formed by migration of oxygen atoms in the lattice.

As shown in Fig. 6c, the asymmetrical O1s spectra of Co/CeO_2-NC catalyst could be decomposed into three components around at BE = 528.9, 529.6 and 531.3 eV. Similarly, O1s spectra of Co/CeO_2-NT catalyst (deconvoluted peaks at 529.1, 530.0 and 531.6 eV) and Co/CeO_2-3DOM catalyst (deconvoluted peaks at 529.5 and 531.3 eV) were present. Deconvoluted peaks below 530 eV could be ascribed to the surface lattice oxygen (O_{latt}). Binding energy between 531.3 or 531.6 eV could be ascribed to the adsorbed oxygen (O_{ads}, e.g. O^{2-}, O_2^{2-} or O^-)[39]. The order of the O_{ads}/O_{latt}(Co/CeO_2-3DOM > Co/CeO_2-NC > Co/CeO_2-NT) was not in agreement with that of the surface oxygen concentration atomic (%) in the Table 3. But it was consistent with H_2-TPR result of H_2 consumption. That can be explained that surface Co atomic concentration (%) of Co/CeO_2-NT catalyst is higher than that of Co/CeO_2-NC catalyst.

As shown in Fig. 6d, Co 2p spectra of three Co/CeO_2catalysts with two main peaks around 780 eV and 796 eV were ascribed to a low intensity satellite of Co $2p_{3/2}$ and a spin-orbit of Co $2p_{1/2}$[35]. The characteristic was further confirmed by XRD results in the Fig. 1b. Compared to Co/CeO_2-NC and Co/CeO_2-NT catalysts, the Co 2p BE (eV) of Co/CeO_2-3DOM catalyst shifted to higher values (780.49 eV), which agrees with the formation of the Co^{n+} between Co and CeO_2-3DOM[40].

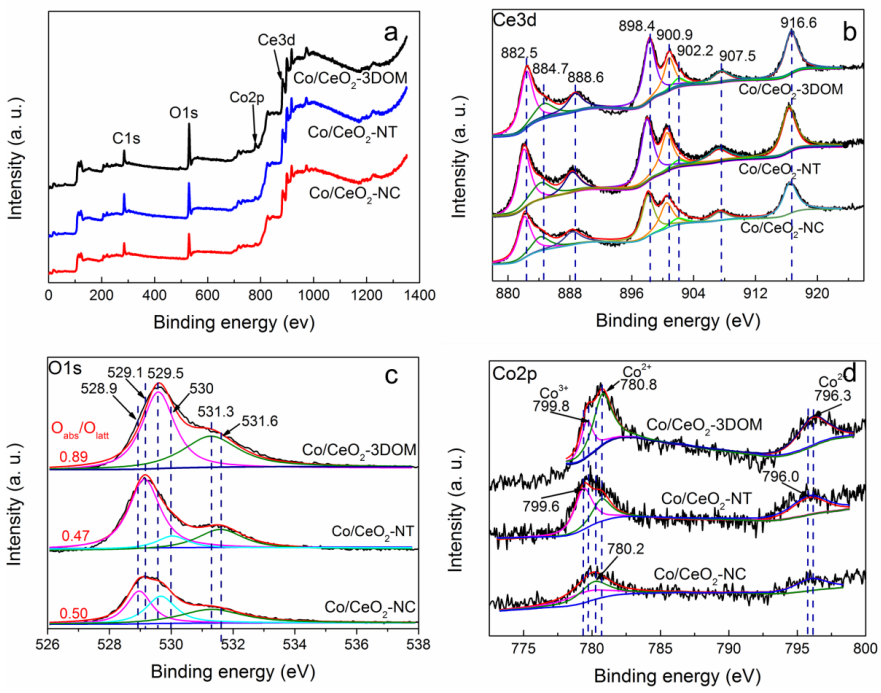

Fig. 6. (a) XPS survey spectra of Co/CeO_2-3DOM, Co/CeO_2-NT and Co/CeO_2-NC catalysts; XPS curve-fitting of the Ce 3d (b), O 1s (c) and Co 2p (d) photoelectron peaks in the Co/CeO_2-3DOM, Co/CeO_2-NT and Co/CeO_2-NC catalysts.

Table 3. Quantities of surface element compositions based on XPS for as-prepared catalysts.

Catalyst	Co 2p BE (eV)	Surface Co concentration atomic %	O_{ads} /O_{latt}	Surface oxygen concentration atomic %	Ce^{3+} /Ce^{4+}
Co/CeO_2-NC	780.03	2.95	0.50	75.31	0.39
Co/CeO_2-NT	779.74	3.26	0.47	76.24	0.33
Co/CeO_2-3DOM	780.49	5.12	0.89	78.50	0.53

3.2 Ammonia decomposition catalytic activity.

The ammonia decomposition reaction ($2NH_3 \rightarrow 3H_2+N_2$ $H = 46$ kJ/mol) of Co/CeO_2-3DOM, Co/CeO_2-NC and Co/CeO_2-NT catalysts were carried out at different temperatures. The results of catalytic activity were showed in Fig. 7. The conversion increased with increasing temperatures is ascribed to endothermic characteristics of ammonia decomposition. The ammonia could be decomposed completely in 600^{o}C for Co/CeO_2-3DOM catalyst. The order of activity for these catalysts was Co/CeO_2-3DOM > Co/CeO_2-NC > Co/CeO_2-NT.

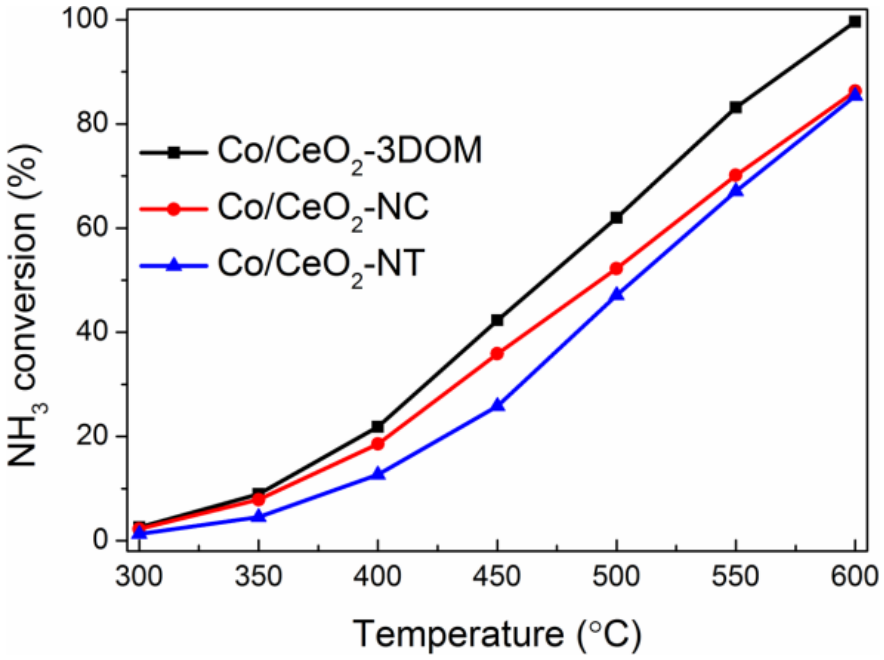

Fig. 7. Ammonia conversion as a function of reaction temperature over Co/CeO_2-3DOM, Co/CeO_2-NC and Co/CeO_2-NT catalysts.

Table 4 summarized the ammonia conversion and H_2formation of Co/CeO_2-3DOM and other typically Co-based catalysts previously reported in the literature[11,20,41-46]. Although the activities of Co/MWCNTs, CoO_x@C-700-A, Co_3O_4 were promoted with mixed oxides and Co/SiO_2 catalysts, showing that their H_2 formation rates are higher than Co/CeO_2-3DOM, the cobalt content of Co/MWCNTs, CoO_x@C-700-A, Co_3O_4 was more than that of Co/CeO_2-3DOM catalyst. In the same cobalt content (5 wt%), the ammonia conversion and H_2formation rate of Co/CeO_2-3DOM catalyst are higher than that of Co/MWCNTs, 5CMAl-2, 5CMCe-2 and $Co/MgO\text{-}La_2O_3$ catalysts. Pfeiffer et al.[41] reported cobalt supported on titanate nanotubes via an ion-exchange method, by which at 550°C, the ammonia conversion of 5CoTi-NT, 10CoTi-NT and 20CoTi-NT catalysts were 23%, 31% and 41%, respectively. In this investigation, the ammonia conversion for cobalt supported on similar CeO_2nanotubes structure was 67%, which is higher than these CoTi-NT catalysts.

Table 4. Ammonia conversion and H_2 formation rate over cobalt based catalysts at 500°C.

Catalyst	Metal content (wt%)	GHSV($ml/g_{cat*}h$)	Ammonia conversion (%)	H_2 formation ($mmol/min{\cdot}g_{cat}$)
Co/CNTs[44]	4.1	5000	8	0.5
Co/MWCNTs[20]	10	6000	74.6	5.0
Co/MWCNTs[51]	5	6000	60	4.0
CoO_x@C-700-A[11]	18.7	15000	55	8.8
Co_3O_4 promoted with mixed oxides[45]	94.8	24000	35	9.4
5CMLa-2[43]	5	6000	48	3.2
5CMCe-2[43]	5	6000	40	2.7
5CMAl-2[43]	5	6000	8	0.5
$Co/MgO\text{-}La_2O_3$[42]	5	6000	60	4.0
Co/SiO_2[46]	66.8	30 000	13	4.3

Catalyst	Metal content (wt%)	GHSV(ml/g_{cat*}h)	Ammonia conversion (%)	H_2 formation (mmol/min·g_{cat})
10CoNaTi-NT[41]	6.8	6000	18	0.35
Co/CeO_2-3DOM	5	6000	62	4.2

As shown in Fig. 8, the Co/CeO_2-3DOM catalyst catalyzed ammonia decomposition for the long lifetime and reusability test between 550-600^{o}C under 6000 mL/g_{cat*}h. It showed that catalytic activity was reproducible in a temperature cycle of 550oC (6 h) to 600oC (18h), then to 550oC (12 h). The excellent catalytic stability and reproducibility of Co/CeO_2-3DOM catalyst could be ascribed to three-dimensional ordered mesoporous structure, which acts as anchoring sites for cobalt active sites and prevents the phenomenon of active site aggregation.

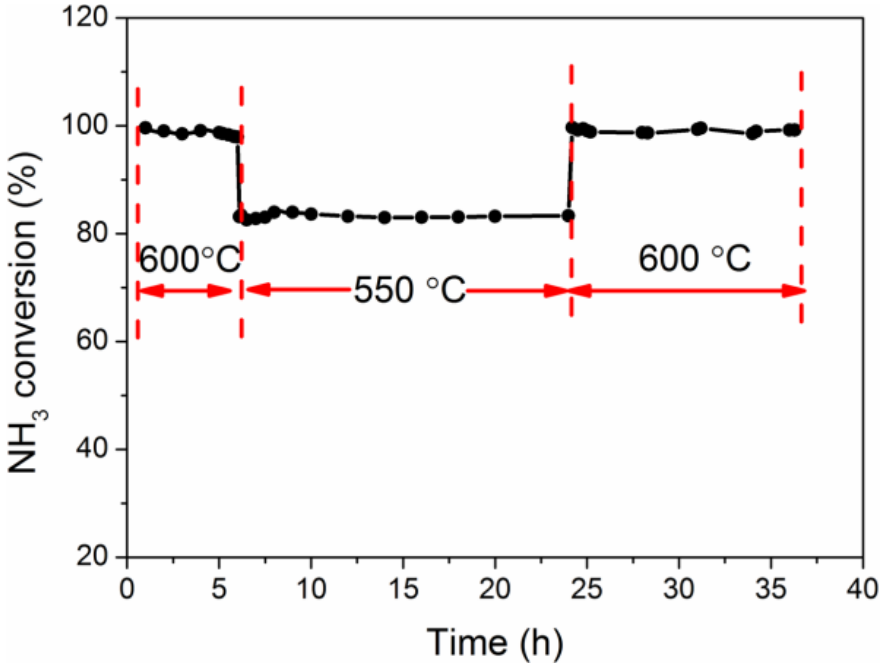

Fig. 8. Time course of ammonia decomposition at 550^{o}C and 600^{o}C using Co/CeO_2-3DOM as a catalyst at GHSV=6 000 mL h^{-1} g_{cat}^{-1}.

The role of different morphology was further verified by the kinetic analysis. The experimental data were evaluated by applying simple power-law kinetics. According to Arrhenius equation($\ln(\text{rate}) = \text{Constant} - \frac{E_a}{R}\frac{1}{T}$), the Arrhenius plots over Co/CeO_2 catalysts were measured in the range of 350-500^{o}C and shown in Fig. 9. It was observed that the Ea value decreased in the order Co/CeO_2-NT (62.31 kJ mol^{-1}) > Co/CeO_2-NC (52.37 kJ mol^{-1}) > Co/CeO_2-3DOM (51.23 kJ mol^{-1}). Su et al.[15] reported that the lowest activation energy of Co nanoparticles inside the tubular channel of carbon nanotubes was 79 kJ mol^{-1}. Comparable to the Co catalyst on different carbons supports[47], the activation energy of Co/CeO_2 catalysts was lower than most of the published Co-based catalysts[41-43].

Fig. 9. The Arrhenius plots for ammonia decomposition over Co/CeO_2-3DOM, Co/CeO_2-NC and Co/CeO_2-NT catalysts.

The reaction mechanism of ammonia decomposition can be explained in following steps: Firstly, ammonia is adsorbed to the active sites and then dissociated into adsorption of N and H atoms. Secondly, N and H atoms recombine in the surface of active sites. Finally, the recombinative N and H atoms desorb from the surface of active sites. The preferred adsorption sites and adsorption energies of NH_x (x = 0-3) and H, and N recombination reactions on the close-packed Fe (110), Co (111) and Ni (111) surfaces were investigated by DFT calculations[48]. Since N desorption is the slowest elementary step of ammonia reaction, it can be observed some accumulation of adsorbed N atoms on the active sites surface, blocking part of the active sites surface. In our previous work[49], electron donating group (such as K^+) as a promoter facilitating electron transfer from support to Ru further facilitates the recombinative desorption of surface N atoms. The electron donation effect of Ce (or oxygen anion vacancy) can weaken the bonding of N adatoms to the Co surface, and then speed the recombinative desorption of N adatoms. This can be described as the following equation (□ represents the oxygen anion vacancy):

$$Ce^{4+}\left(O^{2-}\right)_{2-x}\left(e^{-}\right)_{2x}+Co=Ce^{4+}\left(O^{2-}\right)_{2-x}(\square)_{2x}+Co\left(e^{-}\right)_{2x} \quad (4)$$

Meanwhile, it is well known for Ru-based catalysts that B5-type site, which consists of an arrangement of three Ru atoms in one layer and two other Ru in an internal layer, can enhance catalytic activity for ammonia decomposition[50]. 3d transition metals such as Fe or Co have a similar configuration to the Ru step sites with size around 7 nm rich in B5 sites[25]. Laura et al.[47] suggested that smaller particles were more active than large crystallites in cobalt/carbon catalysts. An approximate cobalt average particle of Co/CeO_2-3DOM catalyst is size of 5.2 nm, which seems to be in agreement with the high activity of the cobalt active sites.

Based on the results of catalytic activity data and the catalyst characterizations, it can conclude that catalytic ammonia decomposition performance of cobalt catalyst depends largely on the structure of the CeO_2 support material and the cobalt particle size. The high performance of the Co/CeO_2-3DOM catalyst for ammonia decomposition is because of the following reasons:

1. Presence of high surface area and high surface cobalt atomic concentration.
2. Three-dimensional order mesoporous CeO_2 supports capable of stabilizing small cobalt nanoparticles.
3. Presence of more surface oxygen vacancies and better Ce^{3+}/Ce^{4+} redox properties compared to other morphology catalysts.
4. Strong metal-support interaction increased transfer electron between cobalt and CeO_2-3DOM support.

4. Conclusion

Different morphology CeO_2 samples with three-dimensional order mesoporous, nanotubes and nanocubes and their supported Co nanocatalysts have been successfully prepared to investigate the morphology-performance relationship for ammonia decomposition. The Co/CeO_2 catalysts from TEM characterization display a nanoparticle structure with an average size of 5.2-7.8 nm. Compared with Co/CeO_2-NT and Co/CeO_2-NC catalysts, the Co/CeO_2-3DOM catalyst possesses the lowest Ea value (51.23 kJ/mol) for ammonia decomposition. The excellent catalytic performance of the Co/CeO_2-3DOM is attributed to the high surface area, more surface oxygen vacancies, strong metal-support interaction, high surface cobalt atomic concentration and smaller particle size. Electronic effect is a critical factor for the high performance of the Co/CeO_2-3DOM catalyst. In addition, the Co/CeO_2-3DOM catalyst shows high stability and superior anti-sintering property during a 36 h lifetime test without deactivation due to the confinement effect of the three-dimensional ordered mesoporous structure. The same strategy can extend to other three-dimensional ordered mesoporous structured oxides, opening a new way for the design of multi-functional nanocatalysts for the ammonia decomposition.

Acknowledgements

This work was supported by the National Natural Science Foundation of China (No. 21868016), the Guangdong Province Natural Science Foundation Project (2018B030315010) , the Hunan Province Key Research and Development Program (No. 2019NCZDNY0005), and the National Key Research and Development Program (No. 2019YFD1002305-3).

Declaration of competing interest

The authors declare no conflict of interest.

References

1. Kojima Y. Hydrogen storage materials for hydrogen and energy carriers. *International Journal of Hydrogen Energy.* 2019;44(33):18179-18192.

2. Schneemann A, White JL, Kang SY, Jeong S, Wan LF, Cho ES, Heo TW, Prendergast D, Urban JJ, Wood BC, Allendorf MD, Stavila V. Nanostructured metal hydrides for hydrogen storage. *Chemical Reviews.* 2018;118(22):10775-10839.

3. Klerke A, Christensen CH, Norskov JK, Vegge T. Ammonia for hydrogen storage: challenges and opportunities. *Journal of Materials Chemistry.*2008;18(20):2304-2310.

4. Giddey S, Badwal SPS, Munnings C, Dolan M. Ammonia as a renewable energy transportation media. *ACS Sustainable Chemistry & Engineering.* 2017;5(11):10231-10239.

5. Lan R, Irvine JTS, Tao S. Ammonia and related chemicals as potential indirect hydrogen storage materials. *International Journal of Hydrogen Energy.*2012;37(2):1482-1494.

6. Schuth F, Palkovits R, Schlogl R, Su DS. Ammonia as a possible element in an energy infrastructure: catalysts for ammonia decomposition. *Energy & Environmental Science.* 2012;5(4):6278-6289.

7. Mukherjee S, Devaguptapu SV, Sviripa A, Lund CRF, Wu G. Low-temperature ammonia decomposition catalysts for hydrogen generation. *Applied Catalysis B: Environmental.* 2018;226:162-181.

8. Ju X, Liu L, Yu P, Guo J, Zhang X, He T, Wu G, Chen P. Mesoporous Ru/MgO prepared by a deposition-precipitation method as highly active catalyst for producing COx-free hydrogen from ammonia decomposition.*Applied Catalysis B: Environmental.* 2017;211:167-175.

9. Su Q, Gu L, Yao Y, Zhao J, Ji W, Ding W, Au CT. Layered double hydroxides derived Nix(MgyAlzOn) catalysts: Enhanced ammonia decomposition by hydrogen spillover effect. *Applied Catalysis B: Environmental.* 2017;201:451-460.

10. Hu Z-P, Chen L, Chen C, Yuan Z-Y. Fe/ZSM-5 catalysts for ammonia decomposition to COx-free hydrogen: Effect of SiO_2/Al_2O_3 ratio.*Molecular Catalysis.* 2018;455:14-22.

11. Li L, Jiang R, Chu W, Cang H, Chen H, Yan J. Cobalt nanoparticles embedded in a porous carbon matrix as an efficient catalyst for ammonia decomposition.*Catalysis Science & Technology.* 2017;7(6):1363-1371.

12. Dasireddy VDBC, Likozar B. COx-free hydrogen generation via decomposition of ammonia over copper and zinc-based catalysts. *Fuel.* 2017;196:325-335.

13. Yi Y, Wang L, Guo Y, Sun S, Guo H. Plasma-assisted ammonia decomposition over Fe–Ni alloy catalysts for CO x-Free hydrogen. *AIChE Journal.*2019;65(2):691-701.

14. Duan X, Ji J, Yan X, Qian G, Chen D, Zhou X. Understanding Co-Mo catalyzed ammonia decomposition: Influence of calcination atmosphere and identification of active phase. *ChemCatChem.* 2016;8(5):938-945.

15. Zhang J, Muller JO, Zheng W, Wang D, Su D, Schlogl R. Individual Fe-Co alloy nanoparticles on carbon nanotubes: structural and catalytic properties.*Nano Letters.* 2008;8(9):2738-2743.

16. Guo J, Wang P, Wu G, Wu A, Hu D, Xiong Z, Wang J, Yu P, Chang F, Chen Z. Lithium imide synergy with 3d transition-metal nitrides leading to unprecedented catalytic activities for ammonia decomposition. *Angewandte Chemie. International Ed. in English.* 2015;54(10):2950-2954.

17. David WIF, Makepeace JW, Callear SK, Hunter HMA, Taylor JD, Wood TJ, Jones MO. Hydrogen production from ammonia using sodium amide. *Journal of the American Chemical Society.* 2014;136(38):13082-13085.

18. Bell TE, Torrente-Murciano L. H_2 production via ammonia decomposition using non-noble metal catalysts: A review. *Topics in Catalysis.* 2016;59(15):1438-1457.

19. Lendzion-Bieluń Z, Pelka R, Arabczyk W. Study of the kinetics of ammonia synthesis and decomposition on iron and cobalt catalysts. *Catalysis Letters.*2009;129(1):119-123.

20. Zhang H, Alhamed YA, Chu W, Ye Z, AlZahrani A, Petrov L. Controlling Co-support interaction in Co/MWCNTs catalysts and catalytic performance for hydrogen production via NH_3 decomposition. *Applied Catalysis A: General.* 2013;464-465:156-164.

21. Ren Y, Ma Z, Bruce PG. Ordered mesoporous metal oxides: synthesis and applications. *Chemical Society Reviews.* 2012;41(14):4909-4927.

22. Montini T, Melchionna M, Monai M, Fornasiero P. Fundamentals and catalytic applications of CeO_2-based materials. *Chemical Reviews.*2016;116(10):5987-6041.

23. Zheng W, Zhang J, Ge Q, Xu H, Li W. Effects of CeO_2 addition on Ni/Al_2O_3 catalysts for the reaction of ammonia decomposition to hydrogen. *Applied Catalysis B: Environmental.* 2008;80(1):98-105.

24. Gong X, Gu YQ, Li N, Zhao H, Jia CJ, Du Y. Thermally Stable Hierarchical Nanostructures of Ultrathin MoS2 Nanosheet-Coated CeO_2 Hollow spheres as catalyst for ammonia decomposition. *Inorganic Chemistry.*2016;55(8):3992-3999.

25. Lucentini I, Casanovas A, Llorca J. Catalytic ammonia decomposition for hydrogen production on Ni, Ru and NiRu supported on CeO_2. *International Journal of Hydrogen Energy.* 2019;44(25):12693-12707.

26. Feng Z, Ren Q, Peng R, Mo S, Zhang M, Fu M, Chen L, Ye D. Effect of CeO_2 morphologies on toluene catalytic combustion. *Catalysis Today.* 2019;332:177-182.

27. Zhang R, Lu K, Zong L, Tong S, Wang X, Feng G. Gold supported on ceria nanotubes for CO oxidation. *Applied Surface Science.* 2017;416:183-190.

28. Xie S, Liu Y, Deng J, Zhao X, Yang J, Zhang K, Han Z, Dai H. Three-dimensionally ordered macroporous CeO_2-supported Pd@Co nanoparticles: Highly active catalysts for methane oxidation. *Journal of Catalysis.* 2016;342:17-26.

29. Chong H, Li P, Xiang J, Fu F, Zhang D, Ran X, Zhu M. Design of an ultrasmall Au nanocluster–CeO_2 mesoporous nanocomposite catalyst for nitrobenzene reduction. *Nanoscale.*2013;5(16):7622-7628.

30. Laha SC, Ryoo R. Synthesis of thermally stable mesoporous cerium oxide with nanocrystalline frameworks using mesoporous silica templates. *Chemical Communications.* 2003(17):2138-2139.

31. Chen G, Sun S, Sun X, Fan W, You T. Formation of CeO_2 nanotubes from $Ce(OH)CO_3$nanorods through Kirkendall diffusion. *Inorganic Chemistry.*2009;48(4):1334-1338.

32. Zhang R, Lu K, Zong L, Tong S. Control synthesis of CeO_2 nanomaterials supported gold for catalytic oxidation of carbon monoxide. *Molecular Catalysis.*2017;442:173-180.

33. López JM, Gilbank AL, García T, Solsona B, Agouram S, Torrente-Murciano L. The prevalence of surface oxygen vacancies over the mobility of bulk oxygen in nanostructured ceria for the total toluene oxidation. *Applied Catalysis B: Environmental.* 2015;174-175:403-412.

34. Huang C, Li H, Yang J, Wang C, Hu F, Wang X, Lu ZH, Feng G, Zhang R. $Ce0.6Zr0.3Y0.1O_2$solid solutions-supported NiCo bimetal nanocatalysts for NH_3 decomposition. *Applied Surface Science.*2019;478:708-716.

35. Bai B, Arandiyan H, Li J. Comparison of the performance for oxidation of formaldehyde on nano-Co_3O_4, 2D-Co_3O_4, and 3D-Co_3O_4 catalysts. *Applied Catalysis B: Environmental.* 2013;142-143:677-683.

36. Yin S, Xu BQ, Wang SJ, Ng CF, Au C. Magnesia–carbon nanotubes (MgO–CNTs) nanocomposite: novel support of Ru catalyst for the generation of COx-free hydrogen from ammonia. *Catalysis Letters* . 2004; 96:113-116.

37. Li X, Ji W, Zhao J, Wang S, Au C. Ammonia decomposition over Ru and Ni catalysts supported on fumed SiO2, MCM-41, and SBA-15. *Journal of Catalysis.*2005;236(2):181-189.

38. Konsolakis M, Sgourakis M, Carabineiro SAC. Surface and redox properties of cobalt–ceria binary oxides: On the effect of Co content and pretreatment conditions.*Applied Surface Science.* 2015;341:48-54.

39. Jaffari GH, Imran A, Bah M, AAli A, Bhatti AS, Qurashi US, Shah SI. Identification and quantification of oxygen vacancies in CeO_2nanocrystals and their role in formation of F-centers. *Applied Surface Science.* 2017;396:547-553.

40. Kim HY, Lee HM, Henkelman G. CO Oxidation mechanism on CeO_2-supported Au nanoparticles. *Journal of the American Chemical Society.*2012;134(3):1560-1570.

41. Lara-García HA, Mendoza-Nieto JA, Pfeiffer H, Torrente-Murciano L. COx-free hydrogen production from ammonia on novel cobalt catalysts supported on 1D titanate nanotubes. *International Journal of Hydrogen Energy.*2019;44(57):30062-30074.

42. Podila S, Driss H, Zaman SF, Alhamed YA, AlZahrani AA, Daous MA, Petrov LA. Hydrogen generation by ammonia decomposition using Co/MgO–La_2O_3 catalyst: Influence of support calcination atmosphere. *Journal of Molecular Catalysis A: Chemical.* 2016;414:130-139.

43. Podila S, Alhamed YA, AlZahrani AA, Petrov LA. Hydrogen production by ammonia decomposition using Co catalyst supported on Mg mixed oxide systems.*International Journal of Hydrogen Energy.*2015;40(45):15411-15422.

44. Zhang J, Comotti M, Schüth F, Schlögl R, Su DS. Commercial Fe- or Co-containing carbon nanotubes as catalysts for NH_3 decomposition.*Chemical Communications.* 2007(19):1916-1918.

45. Lendzion-Bielun Z, Narkiewicz U, Arabczyk W. Cobalt-based catalysts for ammonia decomposition. *Materials.* 2013;6:2400-2409.

46. Yao LH, Li YX, Zhao J, Ji WJ, Au CT. Core–shell structured nanoparticles (M@SiO_2, Al_2O_3, MgO; M=Fe, Co, Ni, Ru) and their application in COx-free H_2production via NH_3 decomposition. *Catalysis Today.* 2010;158(3):401-408.

47. Torrente-Murciano L, Hill AK, Bell TE. Ammonia decomposition over cobalt/carbon catalysts—Effect of carbon support and electron donating promoter on activity. *Catalysis Today.* 2017;286:131-140.

48. Duan X, Ji J, Qian G, Fan C, Zhu Y, Zhou X, Chen D, Yuan W. Ammonia decomposition on Fe(110), Co(111) and Ni(111) surfaces: A density functional theory study. *Journal of Molecular Catalysis A: Chemical.* 2012;357:81-86.

49. Huang C, Yu Y, Yang J, Yan Y, Wang D, Hu F, Wang X, Zhang R, GFeng G. Ru/La_2O_3catalyst for ammonia decomposition to hydrogen. *Applied Surface Science.* 2019;476:928-936.

50. García-García FR, Guerrero-Ruiz A, Rodríguez-Ramos I. Role of B5-type sites in Ru catalysts used for the NH_3 decomposition reaction.*Topics in Catalysis.* 2009;52(6):758-764.

51. Zhang H, Alhamed YA, Al-Zahrani A, Daous M, Inokawa H, Kojima Y, Petrov LA. Tuning catalytic performances of cobalt catalysts for clean hydrogen generation via variation of the type of carbon support and catalyst post-treatment temperature. *International Journal of Hydrogen Energy.*2014;39(31):17573-17582.